Melt inclusion formation during olivine recrystallization: Evidence from stable isotopes

Anne-Sophie Bouvier, Estelle F. Rose-Koga, Alexander R. L. Nichols,
Clémence Le Lay

▶ **To cite this version:**

HAL Id: insu-03708893
https://insu.hal.science/insu-03708893

Submitted on 29 Jun 2022

Melt inclusion formation during olivine recrystallization: Evidence from stable isotopes

Anne-Sophie Bouvier [a],[*], Estelle F. Rose-Koga [b], Alexander R.L. Nichols [c], Clémence Le Lay [a]

[a] *Institut des Sciences de la Terre, Université de Lausanne, Switzerland*
[b] *Laboratoire Magmas et Volcans, Université Clermont Auvergne, France*
[c] *School of Earth and Environment, University of Canterbury, New Zealand*

ARTICLE INFO

ABSTRACT

Melt inclusions are often used to infer melting processes or to determine source magmas that are usually overprinted in bulk rocks due to late stage mixing or near surface contamination. Here we present the first investigation of oxygen (O) isotope equilibrium between melt inclusions and their host olivines from arc samples. Olivines in all but one sample record either magma mixing or fractional crystallization. All six melt inclusions from Vulcano, 83% of seven from Sukumoyama, 44% of 21 from St Vincent, 37% of four from Iwate, and 21% of 13 from Aoba are not in isotopic equilibrium with their olivine host, despite the other major elements being in apparent equilibrium. A detailed study of some of the olivines shows that only a small volume around the melt inclusions is in equilibrium with its host. This strongly suggests that in these olivines melt inclusions are trapped in partly recrystallized olivines, highlighting the importance of magma mixing and crystal recycling in the magmatic plumbing system of these volcanoes. Oxygen isotope fractionation between melt inclusions and their host olivines, as well as phosphorus-$\delta^{18}O$ systematics, could be used to better understand the formation of melt inclusions and crystal history. It could also provide valuable information to help characterize the magmatic plumbing system that the inclusions and their olivine hosts formed in (e.g., crystal rich-mush versus crystal poor melt lenses).

1. Introduction

Olivine-hosted melt inclusions (OHMIs) often record large variations in major, volatile and trace elements that reflect different extents of melting, depths of entrapment or influences from slab fluids on the mantle source (e.g., Kent, 2008). Most data consist of major, trace and volatile elements. Studies reporting stable and radiogenic isotopes measured in melt inclusions are rare (e.g., Koornneef et al., 2019; Maclennan, 2008; Rose-Koga et al., 2012; Saal et al., 2002; Stracke et al., 2019), with only nine reporting oxygen isotopes (Bouvier et al., 2008, 2010, 2019; Gurenko et al., 2001; Gurenko and Chaussidon, 2002; Hartley et al., 2012, 2013; Manzini et al., 2019). Only Manzini et al. (2019) and Gurenko and Chaussidon (2002) report $\delta^{18}O$ in OHMIs and their host olivine. Gurenko and Chaussidon (2002) report that most OHMIs in their Icelandic samples are in O isotopic equilibrium with their hosts. On the contrary, Manzini et al. (2019) show that up to 54% of 32 OHMIs analyzed from an E-MORB sample, and 58% of 21 OHMIs

from an N-MORB sample, both from the mid-Atlantic Ridge, are not in isotopic equilibrium with their host. The range of $\delta^{18}O$ in OHMIs within a single sample reaches 2.6‰, which is far wider than the range measured by laser fluorination in fresh MORB glass (0.5‰; Eiler et al., 2000b) and greater than the SIMS analytical precision (0.3‰, 2 standard deviation, 2SD). The processes that generate the disequilibrium are not yet understood, leading Manzini et al. (2019) to suggest $\delta^{18}O$ data in OHMIs, at least from MORB settings, should be interpreted with caution.

In this study, we present new $\delta^{18}O$ data for olivine crystals from arc settings that contain OHMIs for which $\delta^{18}O$ and $\delta^{37}Cl$ have already been measured (Bouvier et al., 2019). Investigating whether or not the O isotopes in the OHMIs are in equilibrium with O isotopes in their host crystals could help understand the large O isotopic variability that has been measured in OHMIs from a single sample (Bouvier et al., 2019; Manzini et al., 2019). The results, coupled with new trace elements in the OHMIs and their hosts, suggest that a large proportion of the OHMIs analyzed were trapped within remobilized, cumulate olivines. Oxygen isotopes in OHMIs and their host olivine, in addition to being a useful tracer of slab fluids, could give valuable insights into OHMI formation, crys-

* Corresponding author.
E-mail address: anne-sophie.bouvier@unil.ch (A.-S. Bouvier).
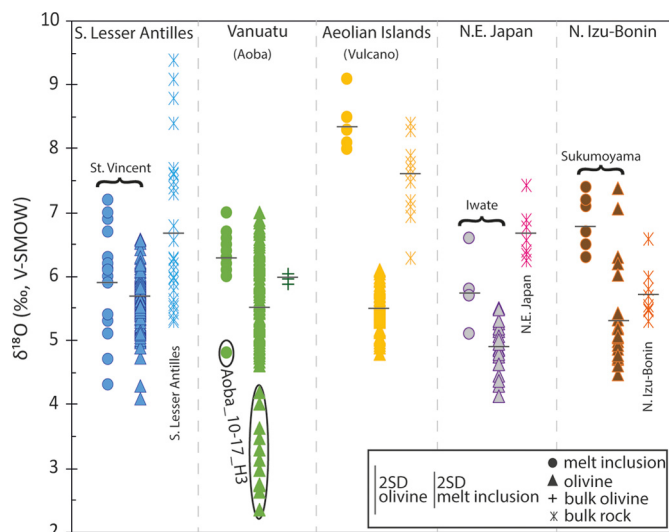
Fig. 1. Comparison of oxygen isotopes measured in OHMIs (Bouvier et al., 2019), their host olivine (this study), bulk olivine (this study) and bulk rock from basaltic magmatic samples from either the same island (Vulcano) or neighbouring volcanic centers from the same arc settings. The bulk rock data are from GEOROC; details can be found in Supplementary Material 2. No bulk rocks from the volcanic front of the Vanuatu arc have been published. The data are thus compared to four bulk olivine measurements performed in this study.

tal history and possibly the magmatic plumbing system in which they formed.

2. Samples

Selected samples were collected from Vulcano (Aeolian Islands, Italy), St. Vincent (Lesser Antilles arc), Iwate Volcano (NE Japan arc), Sukumoyama (Izu-Bonin arc) and Aoba (Vanuatu arc) (Bouvier et al., 2019; Manzini et al., 2017a; Nichols et al., 2012; Rose-Koga et al., 2014). They contain naturally glassy OHMIs that had already been analyzed for major elements, $\delta^{18}O$, as well as $\delta^{11}B$ and $\delta^{37}Cl$ (Bouvier et al., 2019). The OHMIs are basaltic in composition. Their major elements are in equilibrium with those of their host olivine, as reflected by the small amounts of correction for post-entrapment crystallization (mostly <10%; Supplementary Material 1A-B, calculated using Petrolog software; Danyushevsky and Plechov, 2011). Oxygen isotopes in OHMIs ($\delta^{18}O_{MI}$) measured in Vulcano and St. Vincent fall within the range of $\delta^{18}O$ bulk rock values measured in basaltic samples from the literature for Vulcano and Southern Lesser Antilles arc (Fig. 1; Supplementary Material 2). $\delta^{18}O_{MI}$ from Iwate are mostly lower than the $\delta^{18}O$ for bulk rocks from neighbouring volcanic centers, whereas for Sukumoyama $\delta^{18}O_{MI}$ are mostly higher than in the bulk rocks. No bulk rock $\delta^{18}O$ are available for Aoba or from elsewhere along the Vanuatu arc front.

3. Analytical techniques

3.1. SIMS

Oxygen isotopes in olivines have been measured by secondary ion mass spectrometry (SIMS) on a IMS 1280HR at the University of Lausanne, following the same protocol as Manzini et al. (2019) during two separate sessions (September 2018 and September 2019). In brief, a 2nA primary Cs^+ beam was focused on the sample, and secondary ^{16}O and ^{18}O ions were measured on faraday cups in multicollection mode, using a 2460 mass resolution (M/ΔM). A 30 sec pre-sputtering was set at the beginning of each analysis, and total acquisition time was almost 4 minutes per analysis. Four in-house olivine standards were used to calculate the

instrumental mass fractionation as a function of Fo (Mg/(Fe+Mg) mole ratio) content (Supplementary Material 3). The San Carlos olivine in-house standard ($\delta^{18}O = 5.2 \pm 0.12‰$) was measured repeatedly during the session in order to monitor any potential instrumental instability. The repeatability of measurements of the San Carlos olivine standard was 0.37‰ during the first SIMS session and better than 0.30‰ during the second (2 standard deviation, 2SD), which is slightly greater than the statistical error associated with each analysis of the sample olivines (2 standard errors, 2SE). Uncertainty, based on the deviation of $\delta^{18}O$ measured on the San Carlos olivine and the theoretical values of the San Carlos olivine defined by the calibration curve, is 0.4‰ (2SD).

3.2. EMPA

Major elements have been measured in olivine close to each of the spots analyzed for $\delta^{18}O$ by electron microprobe analysis (EMPA) using a JEOL 8200 Superprobe at the University of Lausanne. Conditions were set at 15 kV, 15 nA, using a focused beam of 1 µm. Peak measurement times for Mg, Si, Al, Ti, Ca, Cr, Mn, Fe, Ni were each 30 sec, and 20 sec for Na. Backgrounds were measured for 15 sec. The different elements were standardized using different in-house minerals: fayalite for Si and Fe, forsterite for Mg, wollastonite for CaO, andalusite for Al, rutile for Ti, chromite for Cr, nickel oxide for Ni, tephroite for Mn and albite for Na.

X-rays distribution maps of seven olivines from different samples were acquired using the same electron microprobe. Analytical conditions were 15 kV, 10 nA, with a beam diameter of $\leq$1 µm and 200 ms dwell-time with a 2 µm pixel size for P, Al and Fe.

3.3. LA-ICP-MS

Laser ablation inductively coupled plasma mass spectrometry (LA-ICP-MS) analyses were performed using an Australian Scientific Instruments RESOlution 193 nm ArF excimer laser (including a dual volume sample holder) coupled to a Thermo Element XR sector field ICP-MS via He-Ar carrier gas, at the University of Lausanne. The laser diameter on the sample was 30 or 50 µm (for analysis of olivines) to 10 or 20 µm (for analysis of OHMIs) depending on the size of the MI or available area in the olivine. The repetition rate of the laser was 12 Hz. Elements were measured in the sample for 25 sec, with a fluence of 8 sec. The background was measured before and after the sample for 30 sec. NIST 612 was used as a primary standard, and GOR132 and BHVO were used as secondary standards (Jochum et al., 2006, 2005). Repeatability of all elements on NIST 612 was better than 2% (2SD) over 22 measurements. Uncertainty on the secondary standard varied from 10% (2SD) for the light trace elements up to 28% (2SD) for the heavy trace elements. The data were processed using Iolite software (Paton et al., 2011).

3.4. CO_2-fluorination

Oxygen isotopes were measured at the stable isotope laboratory of the University of Lausanne (Switzerland) using the CO_2 laser fluorination method described in Lacroix and Vennemann (2015). Several analyses of approximately 0.5 – 2 mg were made on four olivines. The samples were pre-fluorinated overnight (min. 10 – 12 h) and subsequently lasered in the presence of about 50 mbar of ultrapure F_2 using a CO_2-laser. The extracted O_2 was purified cryogenically and passed over heated KCl salt. Finally oxygen was absorbed onto a 5 Å molecular sieve and cooled to liquid nitrogen temperature. The O_2 was then analysed with a Thermo Finnigan MAT 253 mass spectrometer. All results are corrected to the NBS-28 quartz standard (9.64‰; Sharp, 1990) and expressed relative to the Vienna Standard Mean Ocean Water. Replicate oxygen isotope analyses of NBS-28 quartz have an average precision of $\pm$0.04‰.

Table 1
Summary of olivine compositions for the different studied samples.

	Fo (%) range	Fo zoning	av. $\delta^{18}O$	2SD	$\delta^{18}O$ zoning	$\delta^{18}O_{core}$-$\delta^{18}O_{rim}$	average $\Delta^{18}O_{OI-MI}$	Equilibrium
St. Vincent, Lesser Antilles								
svn164	84.4 - 88.9	n.d.	6.1	0.37	n.d.		0.9	no
svn184	86.7 - 89.6	n.d.	5.8	0.83	n.d.		−0.9	yes
svn70	77.0 - 89.4	complex	5.6	0.49	no	0.0	−1.0	yes
svn168	86.3 - 89.7	normal	5.8	0.43	no	−0.2	−1.5	no
svn171	75.4 - 85.3	normal	5.7	1.15	lower in the rim	1.2	−1.4	no
							0.6	no
svn36	81.7 - 85.4	n.d.	5.7	0.44	n.d.		−0.2	yes
svn24	84.7 - 88.6	n.d.	5.4	0.36	n.d.		1.2	no
svn181	77.4 - 87.8	complex	5.8	1.05	higher in the rim	−0.8	0.3	no
							−0.4	yes
svn60	83.3 - 86.1	n.d.	5.3	1.11	n.d.		−0.7	yes
svn90	83.4 - 88.3	n.d.	6.0	0.56	n.d.		−0.8	yes
							0.3	no
							0.0	no
svn176	80.2 - 89.2	n.d.	5.9	0.35	n.d.		1.2	no
svn_MM1	80.8 - 85.9	no	5.5	0.59	higher in the rim	−0.7	−0.9	yes
svn_MM3	84.0 - 89.2	complex	5.5	0.41	no	0.3	−0.7	yes
svn_MM2	79.0 - 89.9	n.d.	5.7	0.64	n.d.		−0.7	yes
svn_MM7	78.6 - 88.2	normal	5.6	0.48	no	−0.2	0.2	no
svn_MM15	85.9 - 87.8	n.d.	5.2	0.09	n.d.		−1.0	no
svn_MM22	79.5 - 79.9	n.d.	5.0	0.24	n.d.		−0.4	yes
Aoba, Vanuatu arc								
Aoba_3-1	76.7 - 77.0	no	5.9	0.72	lower in the rim	0.6	−0.6	yes
							−0.3	yes
Aoba_3-4	76.8 - 77.4	normal	5.8	0.73	lower in the rim	0.5	−0.2	yes
Aoba_3-5	77.0 - 79.0	normal	6.0	1.85	lower in the rim	0.7	0.4	no
Aoba_3-6	76.2 - 77.2	no	6.5	0.61	higher in the rim	−0.5	0.1	no
Aoba_3-9	85.0 - 85.9	n.d.	6.4	0.56	n.d.		−0.7	yes
Aoba_3-H1	79.7 - 81.6	no	6.3	0.58	no	−0.1	−0.4	yes
Aoba_10-17-h3	82.5 - 84.4	complex	4.1	2.16	higher in the rim	−1.5	−0.5	yes
Aoba_15-1	84.8 - 87.0	normal	5.3	0.68	no	0.1	−0.9	yes
Aoba_15-10	85.6 - 86.7	no	5.4	0.81	no	0.4	−1.1	no
							−0.5	yes
Aoba_17-10	84.8 - 85.1	normal	5.3	0.65	lower in the rim	0.6	−0.9	yes
Aoba_17-16	86.5 - 86.9	n.d.	5.9	0.38	n.d.		−0.2	yes
Vulcano, Aeolian arc								
S1	90.4 - 90.4	no	5.7	0.06	no	0.0	−2.4	no
S2	90.8 - 91.0	n.d.	5.7	0.51	n.d.		−2.4	no
S3	90.4 - 91.0	n.d.	5.7	0.44	n.d.		−2.2	no
S7	89.9 - 90.6	no	5.3	0.52	no	0.2	−2.9	no
							−3.6	no
S9	89.6 - 89.8	no	5.9	0.30	no	0.1	−2.5	no
Sukumoyama, Izu-Bonin								
Izu_1	83.6 - 85.1	normal	5.0	0.42	no	−0.3	−1.7	no
							−2.0	no
							−2.0	no
Izu_4	80.9 - 84.1	reverse	4.8	0.82	lower in the rim	0.6	−1.7	no
Izu_5	83.6 - 84.6	reverse	6.5	1.22	higher in the rim	−1.4	−1.0	yes
Izu_6	83.3 - 83.8	no	4.9	0.50	lower in the rim	0.6	−1.5	no
Izu_10	83.7 - 84.7	normal	5.5	2.09	higher in the rim	−1.9	−2.5	no
Iwate, NE Japan								
Iwate_1	77.6 - 78.4	normal	5.1	0.34	no	0.3	−1.4	no
Iwate_2	74.9 - 77.0	reverse	4.5	0.50	higher in the rim	−0.5	−1.4	no
Iwate_5	77.4 - 79.2	reverse	5.2	0.63	no	0.2	−0.1	yes
Iwate_10	77.7 - 79.5	no	4.8	1.35	higher in the rim	−0.7		
Iwate_14	77.8 - 79.3	normal	4.9	0.39	no	0.0	−0.9	yes

n.d. (not determined): when no rims were preserved on the grain. There might still be some Fo or $\delta^{18}O$ variation within the grain, often close to the OHMIs or embayments, probably due to Fe diffusion into the olivine.

4. Results

4.1. Olivine major elements compositions

The olivines have forsterite contents (Fo = 100 x Mg/(Fe+Mg)) ranging from 75 to 91. In detail, olivines from Iwate, Sukumoyama and Vulcano have a narrow range of Fo (<5% at each center), whereas Aoba and St. Vincent olivines have more variable Fo (>10%; Table 1). Each sample contains at least one olivine without any apparent Fo zoning. The other olivines display either normal or reverse zoning (Table 1). Three olivines from St. Vincent and one from Aoba display a more complex zoning (core, mantle and rim with non-linear variations in Fo; Supplementary Material 4).

4.2. Olivine $\delta^{18}O$ compositions

At least two $\delta^{18}O$ measurements were made 10-20 μm away from each OHMI in each olivine ($\delta^{18}O_{OI}$), in addition to one in the
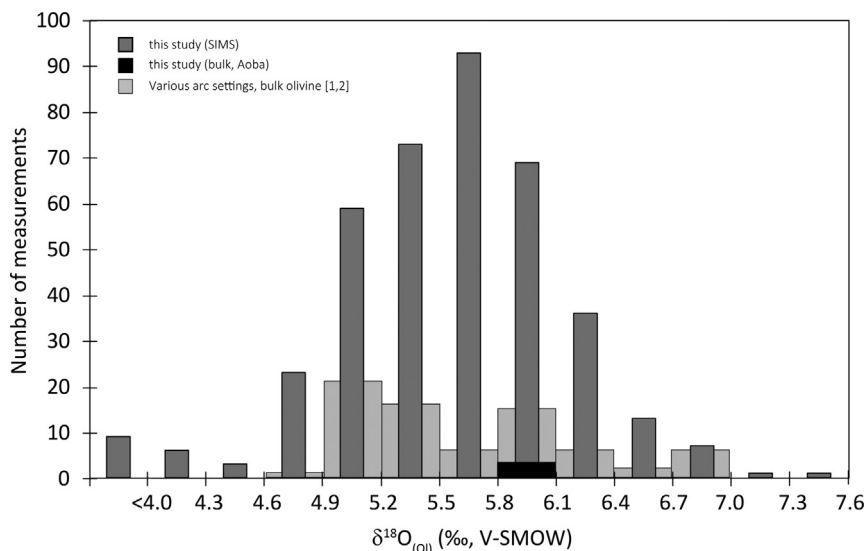
Fig. 2. Histogram of oxygen isotopes measured in olivine. Olivine from this study (SIMS and bulk data) are compared with bulk $\delta^{18}O_{OI}$ from different arc front samples ([1]: Eiler et al., 2000a; [2]: Dorendorf et al., 2000). For SIMS analyses, each olivine has been analysed at least three times for $\delta^{18}O$, whereas bulk measurements consist of at least one olivine analysis. Most of the $\delta^{18}O_{OI}$ from this study range between 5.8 and 6.4‰, as do most of the bulk $\delta^{18}O_{OI}$ from Eiler et al. (2000a) and (Dorendorf et al., 2000). Only olivine from the Kamchatka Arc have bulk $\delta^{18}O > 6.4‰$ (Dorendorf et al., 2000); no $\delta^{18}O < 4.0‰$ have been recorded for bulk olivine from arc front settings, to date.

center of the grain and one at the rim, when a rim was identifiable. In some olivines, spots were also analysed in random locations or as profiles. Results are presented in Fig. 1 and Supplementary Material 5a. Results from the two SIMS sessions give consistent results: of the 11 olivines measured in both sessions, only three have average $\delta^{18}O$ that differ by more than 0.4‰ between both sessions (Supplementary Material 5a). For Aoba_3-10-17-h3 and Aoba_15-1 (Aoba sample (Vanuatu arc), Supplementary Material 6-7), the difference is due to a higher number of olivine analyses revealing heterogeneity in the crystals during the second session. For SVN181 (St. Vincent sample (Lesser Antilles arc), Supplementary Material 4), the reason for the statistically different $\delta^{18}O$ between the two sessions is unclear.

Most of the $\delta^{18}O_{(OI)}$ values measured in this study are between 4.6 and 6.7‰, with the average for each olivine varying from 4.1 to 6.5‰ (Table 1), which slightly extends the range of bulk $\delta^{18}O_{(OI)}$ from the literature (e.g., Dorendorf et al., 2000; Eiler et al., 2000a; Fig. 2) covering a wider range than is typical for bulk olivine from peridotite (+5.2±0.2‰; Mattey et al., 1994). In detail, individual SIMS analyses return values ranging from 2.8 to 7.4‰.

Interestingly, within a sample, $\delta^{18}O_{MI}$ variation is not systematically linked with $\delta^{18}O_{OI}$ variation (i.e., for a given sample, $\delta^{18}O_{OI}$ can vary more or less than $\delta^{18}O_{MI}$; Fig. 1). Overall and within a sample, there is no correlation between $\delta^{18}O_{OI}$ and Fo content of the olivine (Fig. 3). Olivines exhibit varying degrees of $\delta^{18}O_{OI}$ heterogeneity, with 2SD larger than the 2SD of the reference material (Table 1). Only for Vulcano are all the measured olivines homogeneous (2SD <0.5‰; Table 1). For St. Vincent, Aoba and Sukumoyama, olivines are both homogeneous and heterogeneous, with $\delta^{18}O_{OI}$ in the rim higher or lower than that in the core (Table 1). For Iwate, two olivines have higher $\delta^{18}O_{OI}$ in the rim, the remaining are homogeneous (Table 1).

$\delta^{18}O_{OI} > 6.5‰$ (18 data) were mostly measured in rims or close to OHMIs and embayments. Aoba_3 has the most olivines with $\delta^{18}O_{OI} > 6.5‰$ and the highest average $\delta^{18}O_{OI}$, as well as relatively low Fo content (76.8 – 85.9; Table 1) and no bulk rock data. In order to verify these high $\delta^{18}O_{OI}$, four measurements of bulk olivines by CO_2 laser fluorination were made in olivines from sample Aoba_3 to supplement the SIMS measurements of the olivines. The measured bulk $\delta^{18}O_{OI}$ values are similar to the average $\delta^{18}O_{OI}$

Table 2
Bulk oxygen isotopes measurements on olivines from sample Aoba_3.

|	Weight (mg)	$\delta^{18}O$ VMOW
Aoba_3#1	1.93	6.07
Aoba_3#2	1.96	5.90
Aoba_3#3	1.77	5.90
Aoba_3#4	1.60	5.98

Reproducibility of NBS_28 qtz = ± 0.045 ‰ (n = 4).

measured by SIMS in Aoba_3 (average of 6.2‰), but less variable (5.9 – 6.1‰ in bulk compared to 4.9 – 7.0‰ by SIMS, Fig. 1; Table 2).

The most surprising results came from olivine crystal Aoba_3-10-17-h3 which has the most variable $\delta^{18}O$ (2.2‰, 2SD, n = 22), with systematically low values down to 2.4‰. Potential matrix or topography effects were ruled out (Supplementary Material 6). To our knowledge, such low $\delta^{18}O$ values (< 4‰) in olivine have only been reported in ocean island basalts from Mauna Kea (Hawaii; Eiler et al., 2011) and Iceland (e.g., Bindeman et al., 2008, 2006; Eiler et al., 2011; Maclennan et al., 2003), but not yet for arc samples.

4.3. Olivine and melt inclusions trace element compositions

The OHMIs from the five studied arcs are all enriched in fluid mobiles elements (Ba, Pb, Sr) compared to average MORB (Hofmann, 1988), with the strongest enrichment recorded in OHMIs from Vulcano and the weakest enrichment in OHMIs from Iwate (Supplementary Material 1c).

The olivines contain <1 ppm REEs, Sr, Y, Nb and Ba, as expected. Most olivines contain a few ppm (1 – 100 ppm) of P and V. Al, Cr and Ni are the most abundant trace elements in the olivines, with up to 400 ppm Al and Cr, and up to 2800 ppm Ni. Olivines from Aoba and Iwate are more enriched in trace elements compared to olivines from St. Vincent, Vulcano and Sukumoyama. All trace element data are in Supplementary Material 1a and 5b.
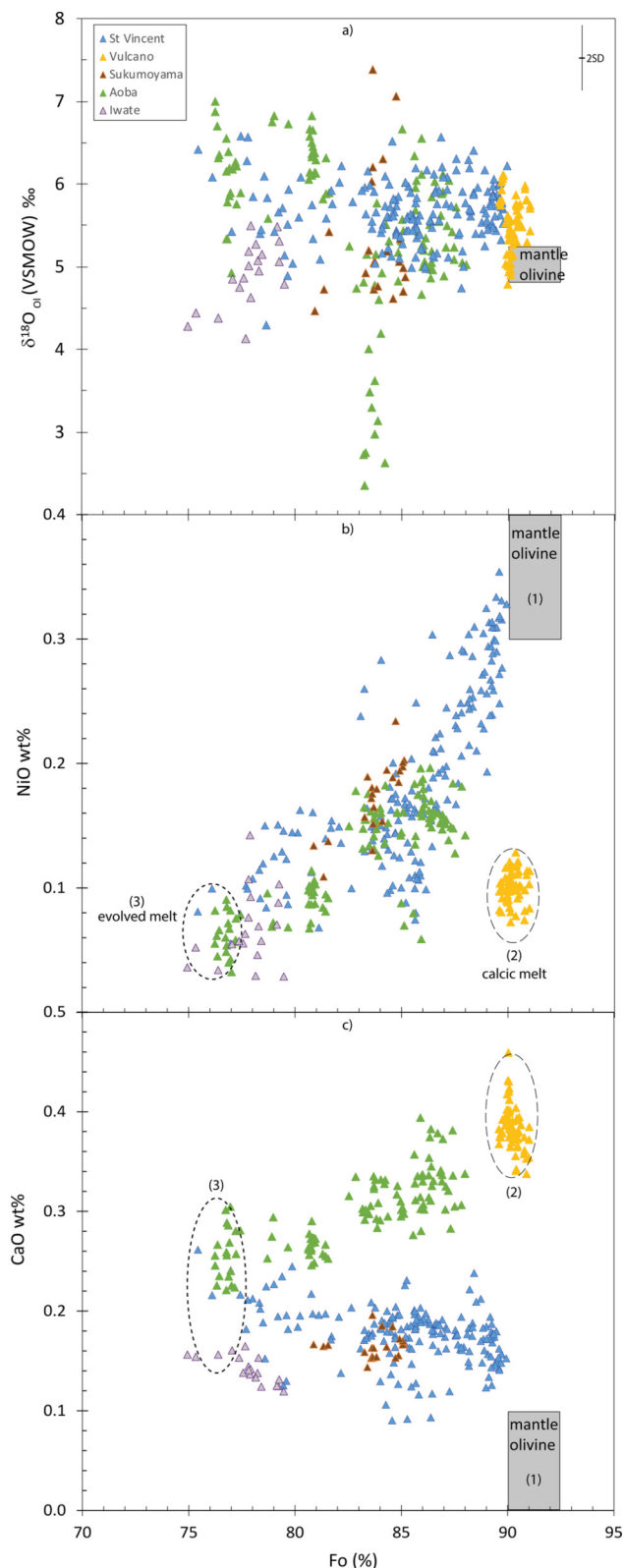
Fig. 3. Forsterite content (Fo = 100x Mg/(Mg+Fe)) compared to a) oxygen isotope composition ($\delta^{18}O_{Ol}$), b) NiO content and c) CaO content of the olivines. The grey field represents bulk mantle olivines (De Hoog et al., 2010; Foley et al., 2013; Mattey et al., 1994). a) No correlation can be seen between $\delta^{18}O_{Ol}$ and Fo content. b and c) Olivines from the five different volcanoes suggest different magmatic histories. St. Vincent, Sukumoyama and Iwate olivines crystallised from a magma derived from a peridotite melt (1). Vulcano olivines are richer in CaO, reflecting the influence of melt from a CaO-rich lithology (2). Finally, Aoba olivines seem to have crystallised from a melt formed by mixing of an evolved peridotite melt (3) with a melt from a CaO-rich lithology.

5. Discussion

5.1. The magmatic history of the olivines

The olivines in this study do not have high enough Fo ($>$90) and NiO ($>$0.3 wt%), and low enough CaO ($<$0.1 wt%) to have originated in the mantle, suggesting a magmatic origin (Fig. 3b-c). The distribution of olivine compositions can be defined by three end-members: 1) Fo $\sim$90, high NiO ($>$0.3 wt%) and low CaO ($\sim$0.12 wt%); 2) Fo $\sim$90, CaO $>$0.4 wt% but low NiO (0.10 wt%); and 3) low Fo, CaO $\sim$0.12 wt% and low NiO (0.04 wt%). Endmember (1) reflects olivine crystallised from a melt derived from mantle peridotite, whereas (3) represents olivine crystallised from an evolved melt derived from the mantle. The second primitive component (2), defined by olivines from Vulcano, represents olivine that has crystallised from ultra-calcic, alkali-rich melts. These melts are interpreted to result from the reaction between hot primitive melts and wehrlitic or gabbroic lithologies at 250 to 350 MPa (Lanzo et al., 2016). Olivines from Aoba seem to form two groups, resulting from mixing between end members (2) and (3). The contribution of both clinopyroxenite and peridotite to the melts beneath Aoba is also reported by Sorbadere et al. (2011).

The variation in Fo content in each olivine crystal provides valuable information on magmatic processes. Normal zoning (a rim with lower Fo) is likely to represent magmatic evolution or magma mixing with a more evolved melt, whereas reverse zoning strongly suggests that the olivine has grown in two different melt compositions, with the second one being more primitive than the melt in which the olivine started growing. These Fo variations can only be preserved if the olivine residence time at high temperature is short (e.g., several years, Costa et al., 2008). All five olivines from Vulcano have homogeneous Fo (intra-grain and grain-to-grain), which either suggests a long residence time that erases Fo zoning or formation of the olivine in a primitive melt with no magma mixing until eruption. Iwate and Sukumoyama olivines have different magmatic histories, reflected by the different types of zoning (reverse or normal). Aoba and St. Vincent olivines are either unzoned or have normal zoning (Table 1), suggesting that some of the olivine retain a record of magmatic evolution. Olivines from Aoba and St. Vincent also display complex zoning, suggesting at least three different magmatic steps.

Fo zoning is not necessarily correlated with $\delta^{18}O$ zoning in olivine (Table 1). This could be explained by the faster interdiffusion of Fe-Mg (e.g., Gaetani and Watson, 2002; Jurewicz and Watson, 1988) in olivine compared to O diffusion at 1250 °C (Dohmen et al., 2002), which could lead to a $\delta^{18}O$ zoning without Fo zoning. This is possibly recorded in olivines SVN_MM1 from St. Vincent, Izu_6 from Sukumoyama and Iwate_10 from Iwate, for which the $\delta^{18}O$ zoning suggest magma mixing, but the absence of Fo zoning either suggests a long residence time or mixing with a melt that has different $\delta^{18}O$ but a similar major element composition. Other olivines have normal Fo zoning, without $\delta^{18}O$ zoning, which can simply be the result of magmatic evolution. Indeed, closed system igneous differentiation is suggested to increase $\delta^{18}O$ up to 0.5‰ in the melt for the range of compositions exhibited by the OHMIs (SiO$_2$ ranging from 44 to 52 wt%), and thus in the crystallizing olivine (e.g., Bindeman, 2008; Bucholz et al., 2017). This could be the case for olivines SVN168, SVN_MM7, both from St. Vincent, Aoba_15-1 from Aoba, Izu_1 from Sukumoyama, Iwate_1 and Iwate_14, both from Iwate. Of all the olivines analysed, only one (Iwate_5 from Iwate) with reverse Fo zoning has no $\delta^{18}O$ zoning, which cannot result from magmatic differentiation. Instead, it could have resulted from mixing between magmas with similar $\delta^{18}O$. Many olivines have preserved normal or reverse zoning as well as $\delta^{18}O$ zoning (two olivines from St. Vincent, SVN171, SVN181; three from Aoba, Aoba_3-4, Aoba_3-5, Aoba_17-
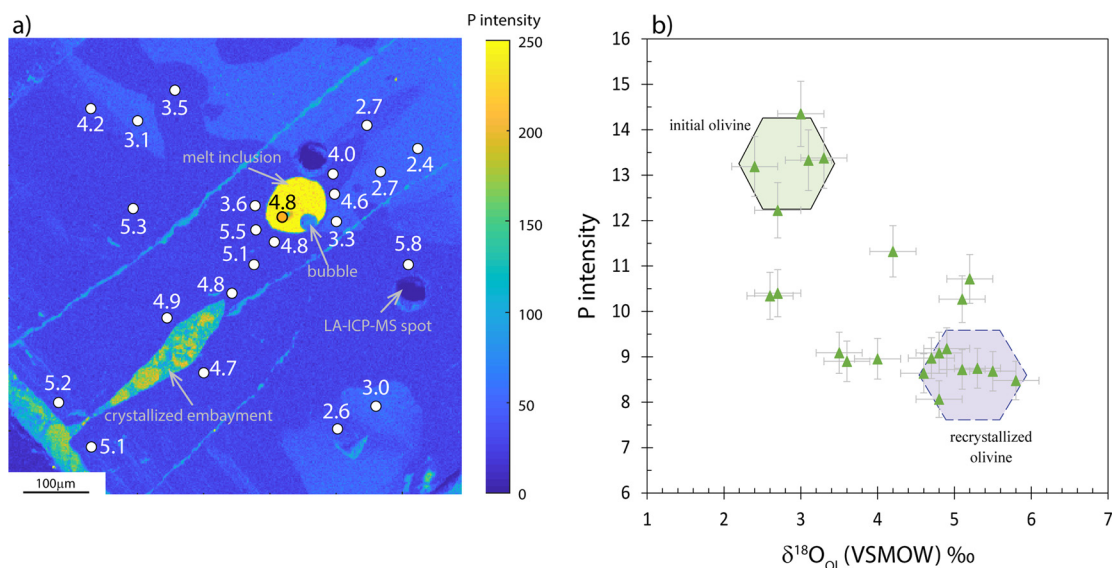
Fig. 4. a) X-ray map of phosphorus in olivine crystal Aoba3_10-17-h3 showing an OHMI and microcrystallized melt embayment. The colour scale shows the intensity of the phosphorus count rate. Different phosphorus zones can be seen, reflecting dissolution textures. The OHMI is enriched in phosphorus compared to the crystallized melt embayment. Several $\delta^{18}O$ measurements have been made in the olivine (white dots). Phosphorus-depleted areas tend to have higher $\delta^{18}O$ than the areas of olivine more enriched in P. The latter have highly depleted $\delta^{18}O$ (area with a minimum of $+2.4‰$) compared to typical upper mantle values ($+5.5 \pm 0.3‰$, e.g., Eiler, 2001), possibly reflecting local assimilation of material altered at the time this domain of the olivine formed. b) Plot of phosphorus intensity (derived from XMapTools, Lanari et al., 2019) compared to individual SIMS analyses of the olivine crystal Aoba3_10-17-h3. The correlation between phosphorus intensity and $\delta^{18}O_{Ol}$ is highlighted, showing the possible initial olivine (green hexagon) with lowest $\delta^{18}O$ and highest phosphorus intensity, and the reverse for the recrystallized olivine (blue hexagon). Some measurements fall in between these two extreme compositions, either reflecting mixing or olivine heterogeneity. (For interpretation of the colours in the figure(s), the reader is referred to the web version of this article.)

10; three from Sukumoyama, Izu_4, Izu_5, Izu_10; and one from Iwate, Iwate_2) that records magma mixing. In summary, in all samples except those from Vulcano, a few olivines have preserved a record of normal magmatic evolution and most of them record magma mixing.

5.2. Significance of the extreme $\delta^{18}O$ values measured in olivines

5.2.1. Origin of the low $\delta^{18}O_{Ol}$

Twenty-one SIMS analyses of olivines have $\delta^{18}O_{Ol}$ values $\leq 4.6‰$; these are the lowest values that have been reported for arc front settings, to date (Fig. 2). These values have been found in seven different olivine crystals, in both cores (e.g., olivines Aoba_3-10-17-h3, Iwate_2, Izu_4, Iwate_10) and rims (e.g., olivines Izu_6 and SVN171). All the $\delta^{18}O_{Ol}$ analyses $\leq 4.6‰$ are associated with olivines that have Fo <84, which is usually interpreted as reflecting crystallization in a melt affected by assimilation of low $\delta^{18}O$ crustal material altered at high temperature (e.g., Genske et al., 2013; Wang and Eiler, 2008). For olivines from Iwate, there is a weak positive relationship between Fo and $\delta^{18}O_{Ol}$ (Fig. 3a), suggesting mixing between a moderately mafic melt (with olivines Fo$_{80}$) with mantle-like $\delta^{18}O$, and a more evolved (leading to olivine Fo$_{75}$) melt with $\delta^{18}O$ ~4.5‰. On the contrary, for olivines from Aoba, Sukumoyama and St. Vincent, no correlation is observed between Fo and $\delta^{18}O_{Ol}$, suggesting that for those volcanoes the volume of low $\delta^{18}O$ in the system is very small. The olivine crystal Aoba_3-10-17-h3 with the lowest $\delta^{18}O_{Ol}$ measured in this study (2.4‰) has preserved evidence of olivine dissolution, as observed in the zoning of phosphorus (Fig. 4). The phosphorus zones are not correlated with Fo zones (Supplementary Material 6), but rather with $\delta^{18}O$. Indeed, the lowest $\delta^{18}O_{Ol}$ are measured in the crystal domains with the highest phosphorus (340 ppm, Supplementary Material 5). The correlation between low $\delta^{18}O_{Ol}$ and high phosphorus domains (>1000 ppm) in a Mauna Kea olivine led Eiler et al. (2011) to suggest that oxygen isotope fractionation between olivine and the melt might be affected by the olivine growth rate. The high phosphorus domains, due to diffusion-limited growth,

usually have phosphorus content higher than 1000 ppm and are limited to narrow bands of a few microns (e.g., Manzini et al., 2017b; Milman-Barris et al., 2008). However, in the specific case of Aoba_3-10-17-h3, dissolution textures are evident and the high phosphorus zones do not resemble typical diffusion-limited growth. Instead, the high phosphorus zones with low $\delta^{18}O$ reflect olivine that was partially dissolved. Reprecipitated olivine has lower phosphorus (8 ppm, Supplementary Material 5), as observed in other studies (e.g., Manzini et al., 2017b; Milman-Barris et al., 2008) and higher $\delta^{18}O$ (~5‰), reflecting crystallization in a melt with a different $\delta^{18}O$ than the one in which olivine initially grew.

The initial low $\delta^{18}O_{Ol}$ values in Aoba3_10-17-h3, in the high phosphorus zone, with a relatively evolved composition (Fo$_{83-84}$), could reflect local mixing with a melt of crust that was hydrothermally altered at high temperature. The presence of a crater lake at Aoba may help fluids circulate locally to great depth (e.g., Warden, 1970), although there are other volcanoes with a crater lake that do not have evidence of low $\delta^{18}O$ melt (e.g., Deegan et al., 2021). The olivine is subsequently remobilized by a melt with $\delta^{18}O$ of around 5.2-5.5‰ as recorded in the rim and possibly more primitive as recorded in the trapped OHMI. The recrystallized olivine has a mixed $\delta^{18}O_{Ol}$ composition between the initial low $\delta^{18}O$ and the more mantle-like $\delta^{18}O$. This could explain the relatively low $\delta^{18}O$ (4.8‰), for an island arc setting, of one of the Aoba OHMIs, even though it has typical major and trace element compositions (e.g., Fig. 5; Supplementary Material 1), and suggests that this OHMI was trapped during recrystallization of a remobilized olivine. This is the only olivine of the six that were mapped with such features (Supplementary Material 8), and the only crystal of those that have been analysed with $\delta^{18}O_{Ol}$ $<4‰$, suggesting that olivine growth in a low $\delta^{18}O$ melt, possibly reflecting localized crustal assimilation by high temperature fluids, and dissolution-reprecipitation due to remobilization by a more mafic melt is rare.

5.2.2. Origin of the high $\delta^{18}O_{(Ol)}$

High $\delta^{18}O_{Ol}$ values ($>6.0‰$) are relatively unusual (e.g., Fig. 2), but have already been reported in olivines from Kamchatka, mea-
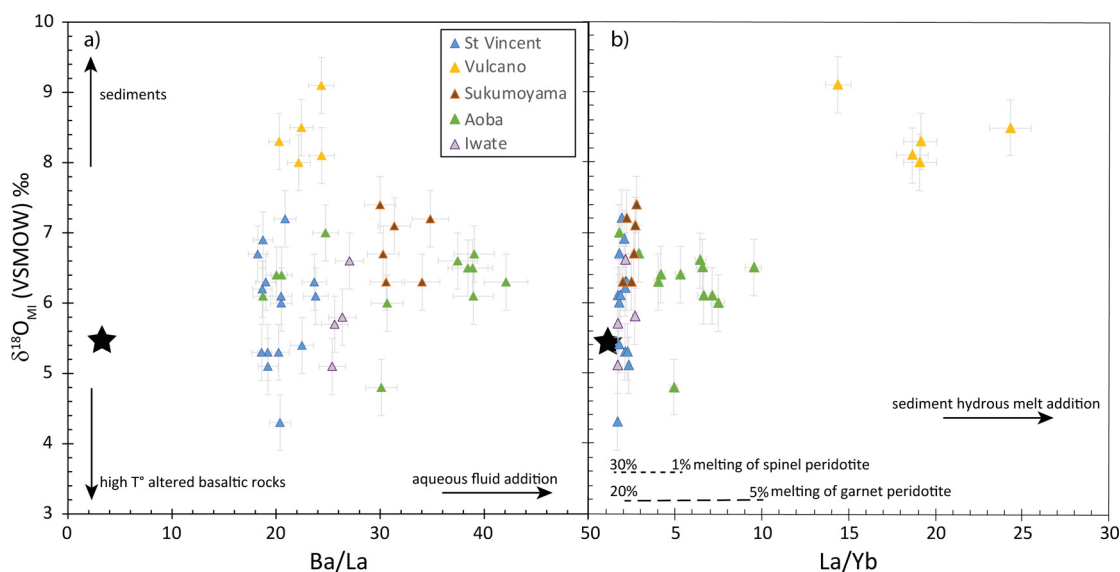
Fig. 5. Oxygen isotopes ($\delta^{18}O_{MI}$) compared to a) Ba/La and b) La/Yb in OHMIs. Symbols are the same as in Fig. 4. Error bars on each symbol represent the propagated error of a single $\delta^{18}O_{MI}$ measurement ($\leq 0.2\permil$, 2se) and of the accuracy of the glass calibration (0.3 – 0.4‰, 2SD; Bouvier et al., 2019). Black stars represent the average N-MORB compositions (e.g., Hofmann, 1988; Eiler et al., 2000a). (a) All OHMIs are enriched in Ba/La compared to N-MORB, suggesting influence from a hydrous component, mostly driving $\delta^{18}O$ towards higher values than MORB. (b) OHMIs from St. Vincent, Iwate and Sukumoyama have La/Yb comparable to MORB, suggesting the hydrous component is aqueous fluids; whereas Aoba and Vulcano OHMIs contain significantly higher La/Yb, suggesting the influence of a hydrous sediment melt instead of aqueous fluids. Melting curve estimates suggest a spinel lherzolite with 0.578 olivine, 0.27 opx, 0.119 cpx and 0.33 sp, and garnet lherzolite with 0.598 ol, 0.211 opx, 0.076 cpx and 0.115 grt. Partition coefficients have been taken from GERM database.

sured either by CO_2 or ArF laser techniques (Auer et al., 2009; Dorendorf et al., 2000; Fig. 2). They are interpreted as resulting from hydrous melt fluxing of mantle wedge peridotite that has interacted with a shallow metasomatized high-$\delta^{18}O$ lithospheric mantle.

Bouvier et al. (2019) suggested that the high $\delta^{18}O_{MI}$ ($>6.5\permil$) preserved in the OHMIs from this study, coupled with low $\delta^{37}Cl$ ($<-1.5\permil$), reflect the imprint of subducted sediments. Indeed, $\delta^{18}O$ of sediments vary from 8 to 30‰ (e.g., Bindeman, 2008) and strongly negative $\delta^{37}Cl$ are usually attributed to the influence of sediments (e.g., Barnes and Sharp, 2017). Sediment influence beneath St. Vincent, Aoba, Vulcano, Iwate and Sukumoyama has also been proposed by other studies based on traces elements and/or stable isotopes (e.g., Bouvier et al., 2008; Manzini et al., 2017a; Métrich and Deloule, 2014; Nichols et al., 2012; Peccerillo et al., 2013; Rose-Koga et al., 2014).

Fractionation of $\delta^{18}O$ at high temperature ($>500\,°C$) is relatively small in silicate minerals ($<2\permil$, Zheng et al., 1999), so it is estimated that the bulk sediment melt and aqueous fluids have similar $\delta^{18}O$. The nature of the sediment component (aqueous vs. melt-like fluid) could not be determined based solely on the isotopic data. Trace elements ratios can help identifying the nature of the fluids, for example using fluid tracers, such as Ba/La (Ba being a fluid mobile element), or the ratio of fluid immobile elements, such as La/Yb. Ba/La in the studied samples show that their primitive melts have been modified by an aqueous fluid addition, as all OHMIs have higher Ba/La than MORB (Fig. 5a). La/Yb can be affected by different degrees of melting, the nature of the mantle source (e.g., garnet or spinel lherzolite) and input of hydrous melt from sediments. $\delta^{18}O_{MI}$ and Ba/La do not correlate within each sample (Fig. 5a), but the relatively stable La/Yb ratios, similar to MORB, for St. Vincent, Iwate and Sukumoyama strongly suggest that the sediment contribution is made via aqueous fluids at these volcanoes (Fig. 5b). On the contrary, Aoba and especially Vulcano both have higher Ba/La than MORB but also significantly higher La/Yb. Different degrees of melting of a mantle source alone cannot explain the La/Yb variations for Aoba and Vulcano, but instead suggest that the sediment imprint originates from a hydrous melt-

like component at these two volcanoes. Thus high $\delta^{18}O_{Ol}$ ($>6.0\permil$) measured in the samples from this study record a contribution from the slab to the mantle melting, possibly in the form of a hydrous melt of the sediment.

### 5.3. Oxygen isotope disequilibrium between melt inclusions and their host olivine

First, it has to be noted that equilibrium fractionation of MORB ($\Delta^{18}O_{Ol-MI} = -0.58\permil$ at $1250\,°C$) or alkali basalts ($\Delta^{18}O_{Ol-MI} = -0.44\permil$ at $1250\,°C$), both calculated based on the equation $1000\ln\alpha = 10^6 A/T^2$, with A coefficient for olivine-melt from Matthews et al. (1998), cannot be distinguished by individual SIMS measurements (accuracy of 0.4‰). These calculated values are close to $\Delta^{18}O_{Ol-MI}$ values measured, for example, by Eiler (2001) or Gurenko and Chaussidon (2002). Similarly, a difference in temperature from 1300 to $1000\,°C$ during crystal growth would lead to less than 0.3‰ variation in $\delta^{18}O$ (e.g., Bindeman, 2008; Eiler, 2001), which is also unresolvable by SIMS. A large proportion of the olivine-OHMI pairs significantly deviate from the theoretical equilibrium for $\delta^{18}O$ ($> 0.5\permil$, Fig. 6). The measured $\Delta^{18}O_{Ol-MI}$ span a large range, from -3.8 to $+1.4\permil$ (Fig. 7). The disequilibrium between the olivine and OHMIs is not linked to the composition of the olivine, as no relationship could be seen between $\Delta^{18}O_{Ol-MI}$ and Fo% (Fig. 7). This excludes any potential analytical artefacts or potential effects on oxygen isotopes during magmatic evolution. Oxygen isotope values in all six OHMIs from Vulcano are in disequilibrium with their host, whereas for St. Vincent, Aoba, Iwate and Sukumoyama variable proportions (46% of 21, 79% of 13, 63% of four and 17% of seven, respectively) of the OHMIs are in equilibrium with their host (Fig. 7). Most $\Delta^{18}O_{Ol-MI}$ for Aoba and St. Vincent and two from Iwate are >0, which is not permitted by the equilibrium equation.

Oxygen isotopic disequilibrium between OHMIs and their host could theoretically result from O diffusion during or after entrapment. As oxygen diffuses slowly in silicate melts (Lesher et al., 1996), with ^{16}O diffusing faster than ^{18}O (Lesher, 2010), the formation of a boundary layer could lead to higher $\delta^{18}O$ in the remaining
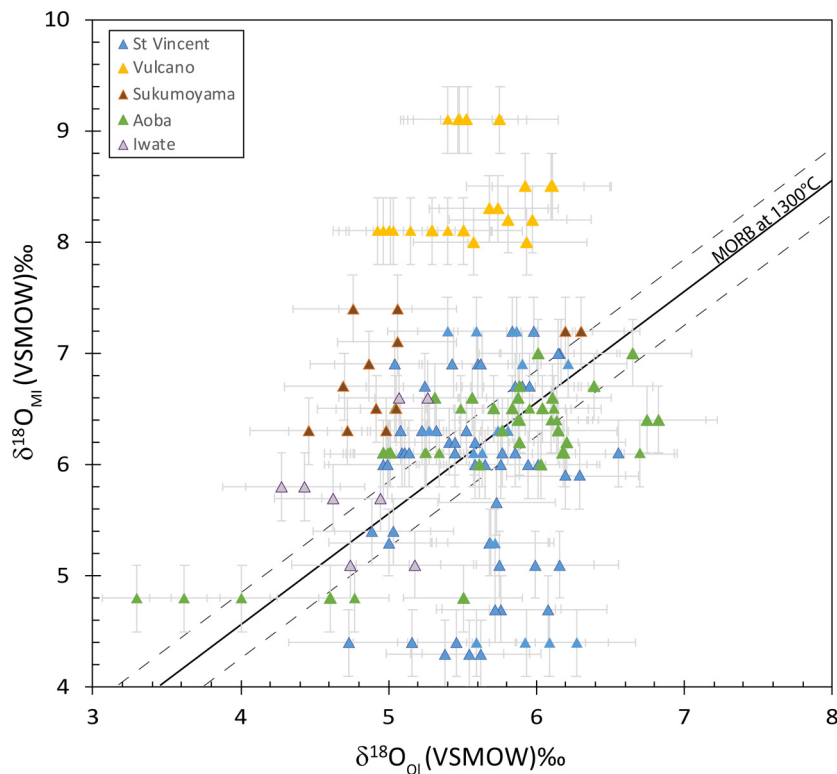
Fig. 6. $\delta^{18}O_{Ol}$ plotted against $\delta^{18}O_{MI}$. MORB theoretical equilibrium is represented by the black line, (calculation described in the main text). Dashed lines show error of $\pm 0.4‰$. Each point represents a single olivine measurement associated with the $\delta^{18}O$ of the OHMI, meaning that there is at least two data points per OHMI. A significant proportion of the olivine-OHMI pairs deviate from the theoretical equilibrium.
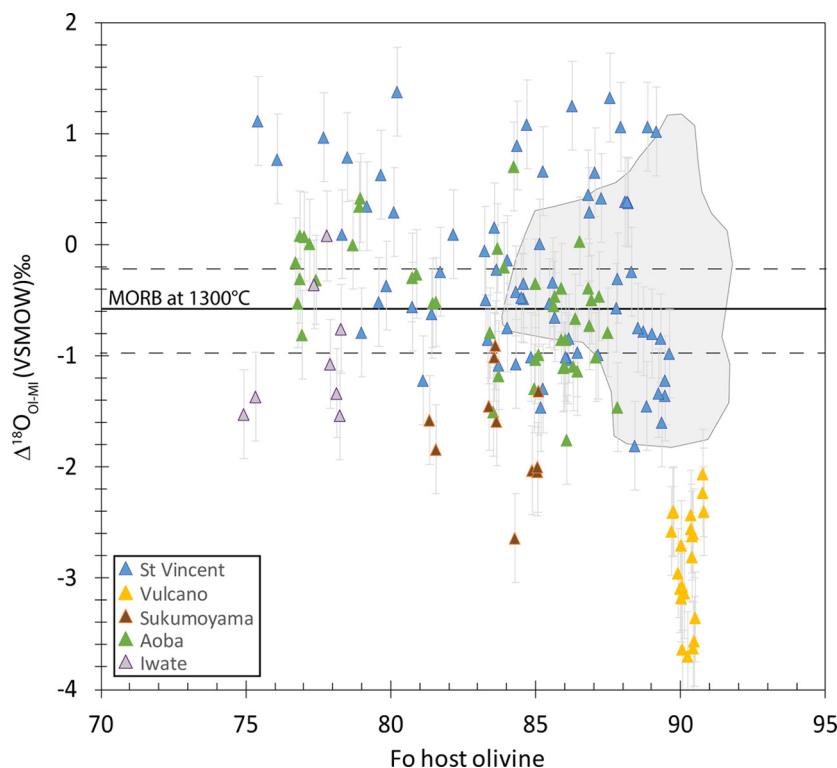

Fig. 7. Comparison of $\Delta^{18}O_{Ol-MI}$ ($\delta^{18}O_{Ol} - \delta^{18}O_{MI}$) with the Fo content of the host olivines. Each point represents one olivine measurement compared to a MI it hosts. The error bars indicate the propagated error of 2 standard errors for $\delta^{18}O_{Ol}$ and $\delta^{18}O_{MI}$. For each OHMI, its olivine host has been measured twice within 100 µm of the edge of the OHMI in different directions. Thus, there are several $\Delta^{18}O_{Ol-MI}$ for each OHMI. Theoretical equilibrium for MORB at 1300 °C is represented by the black lines (based on Matthews et al., 1998) and the dashed lines represent the SIMS uncertainty. The grey field shows the range of $\Delta^{18}O_{Ol-MI}$ in MORBs for comparison (Manzini et al., 2019). At a given Fo content, there is a large range of $\Delta^{18}O_{Ol-MI}$ among the arc samples analyzed here. OHMIs from Vulcano have the lowest $\Delta^{18}O_{Ol-MI}$ compared to equilibrium values, whereas St Vincent OHMIs have the highest $\Delta^{18}O_{Ol-MI}$. St. Vincent, Aoba and Iwate OHMIs have both higher and lower $\Delta^{18}O_{Ol-MI}$. Processes able to generate the disequilibrium are discussed in the main text.

(shrinking) OHMIs compared to the melt in which the host crystal is growing. Boundary layer effects should thus shift $\Delta^{18}O_{Ol-MI}$ towards lower values compared to equilibrium. In fact, all Vulcano OHMIs have $\Delta^{18}O_{Ol-MI}$ much lower than equilibrium (lower than $-2.4‰$; instead of between $-0.5‰$ and $-0.44‰$, at equilibrium) due to higher $\delta^{18}O$ of the MI. But if the development of boundary layers affected the Vulcano OHMI compositions, partitioning of slow diffusing incompatible elements such as phosphorus and Y between the OHMIs and their host should be far higher in Vulcano OHMIs than in the OHMIs from the other volcanoes. However, Vulcano OHMIs have similar partition coefficients (K_d) for phosphorus and Y compared to other OHMIs (Supplementary Material 1a). Also, for St. Vincent and Aoba OHMIs, for which $\Delta^{18}O_{Ol-MI}$ are both higher and lower than equilibrium, there is no correlation between K_d of incompatible elements and $\Delta^{18}O_{Ol-MI}$, suggesting that the lower $\Delta^{18}O_{Ol-MI}$ do not result from a boundary layer effect in these samples. Similarly, the lack of a correlation between the size of the OHMIs and the ratio of incompatible elements with very different diffusion rates, such as K_2O/TiO_2 (e.g., Kress and Ghiorso, 1995), confirms the absence of a boundary layer (Supplementary Material 1d).

Oxygen diffusion from the OHMI to the host olivine after entrapment should lead to higher $\delta^{18}O$ in the OHMI and lower $\delta^{18}O$ in the surrounding olivine. This might also result in a lower $\Delta^{18}O_{Ol-MI}$ compared to equilibrium. Because oxygen is a slow diffuser (Lesher et al., 1996) and the olivine and melt contain similar amounts of O, diffusion of O along a chemical gradient should be negligible. Thus, neither boundary layer effects nor post-entrapment O diffusion could explain the $\Delta^{18}O_{Ol-MI} > 0$ values.

Disequilibrium could be explained if an olivine trapped a different melt than the one in which it initially grew. This could happen during magma mixing and olivine remobilization. These scenarios are illustrated in Fig. 8. Initially, an olivine crystallizes deep in the magmatic plumbing system, trapping melt inclusions (Fig. 8B). During ascent, the olivine enters the upper lens. Partial dissolution of the crystal edges will create reentrants in the olivine filled by a melt that is a mixture of the lower lens and upper lens melts, or only the upper lens melt if olivine has started to partially dissolve during ascent. The olivine resumes its growth, trapping a melt inclusion with different $\delta^{18}O$ than the first melt inclusions (Fig. 8B). In the second scenario (Fig. 8C) the olivine is remobilized. Petrological and geochemical observations have shown that crystals can be remobilized by ascending melts (e.g., Cashman et al., 2017; Lange et al., 2013; Wieser et al., 2019). This would lead, for example, to reverse zoning in some olivines if the crystals had been remobilized by a more mafic melt, as observed in olivines Izu_4, Izu_5, Iwate_2 and Iwate_5 from Sukumoyama and Iwate. During olivine remobilization, the new melt may dissolve the olivine along defects or interact with the previous melt at reentrants of the crystal. Olivine crystallization will resume again trapping melts with a different composition to the melt in which the host crystal initially grew. Such a scenario is compatible with olivine Aoba_3-10-17-h3 (Fig. 8D). Indeed, this olivine crystallized with low $\delta^{18}O$ due to localized interaction with a low $\delta^{18}O$ magma. The olivine was remobilized by the arrival of a new hotter, possibly wetter, melt resulting in its partial dissolution (possibly enhanced by decompression). Olivine re-crystallizes with a composition that is a mixture between the uncontaminated melt and the initial olivine composition.

If an olivine trapped a melt with a different $\delta^{18}O$ composition to the initial melt in which it grew, the olivine around the inclusions should be in equilibrium with the melt. For example, Gurenko and Chaussidon (2002), in a study on Icelandic basalts found that only a 100 μm layer of olivine around the OHMI was in equilibrium with the OHMI. In this study, six of the olivines that were found to be in apparent disequilibrium with their OHMIs
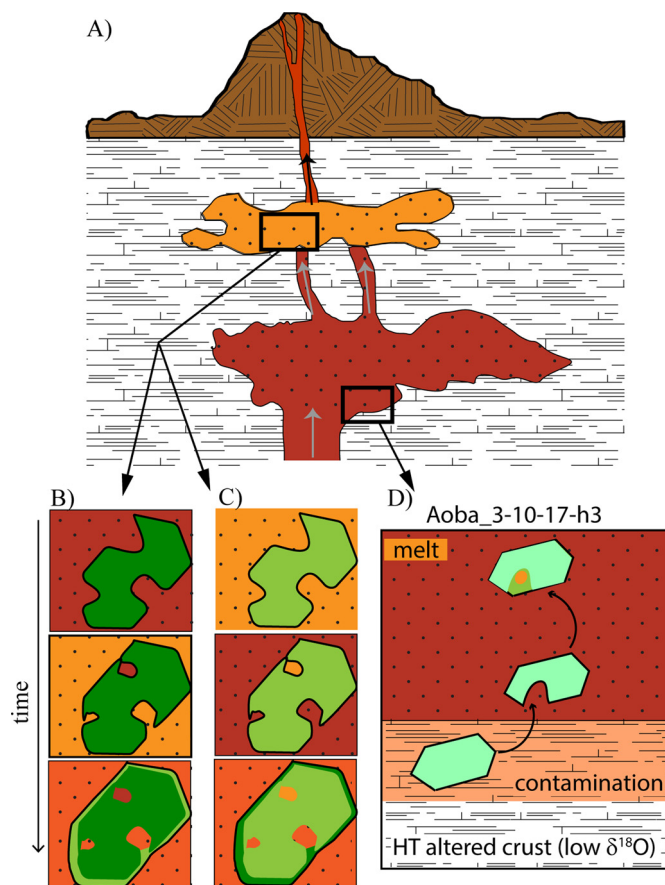
Fig. 8. Simplified conceptual model of a magmatic plumbing system, based on $\delta^{18}O$ measured in olivine and their melt inclusions. None of the cartoons are to scale. A) A simplified magmatic system with two melt lenses. Grey arrows symbolize the arrival of a new, possibly hotter melt, with potentially different $\delta^{18}O$ and/or major element compositions (symbolized by a darker colour) to the upper lens. B) Evolution of an olivine crystallizing in the deeper lens, trapping melt inclusions inside a single crystal that are a mixture of melt from the lower and upper lenses. C) An olivine that crystallizes or is stored in the upper lens. The arrival of the new, possibly hotter melt, with potentially different major element and $\delta^{18}O$ composition could potentially dissolve the olivine and result in melt inclusions that are a mixture of melt from the lower and upper lenses being trapped inside a single crystal. D) A cartoon summarizing a possible scenario for Aoba_3-10-17-h3: an olivine crystallized with low $\delta^{18}O$ due to local contamination by altered crust. See main text for more details.

during the first SIMS session were selected to find possible olivine domains around the OHMIs that were in isotopic equilibrium (Supplementary Material 6-7). Half of them showed a small olivine domain (50 – 60 μm) around the melt inclusions that is in equilibrium with the OHMIs, suggesting that these inclusions have been trapped in an olivine during its remobilization by a melt with a different $\delta^{18}O$ composition. For the other olivines, it is possible that the olivine domain in O isotopic equilibrium with the OHMI has been polished away, could be below the surface or is smaller than the SIMS beam size (<10 – 15 microns). In the OHMIs with only two olivine measurements, those with a large reproducibility (>0.4‰) most likely reflect that the melt inclusions formed in a partly recrystallized olivine. Overall, assuming that all the OHMIs in apparent disequilibrium have been trapped in a recrystallized olivine, ~70% of the studied OHMIs have been trapped during magma mixing.

5.4. Implications

Episodic recharge of melt pockets or magma chambers is widely recognized as a possible trigger for volcanic eruptions (e.g., Sparks

et al., 1977). The proportion of remobilized and partly recrystallized crystals could provide valuable information about the plumbing system of a volcano: a high proportion of remobilized olivine suggests a high proportion of crystals in the last melt pocket, or that the ascending melt has scavenged crystals from different melt pockets as it ascended.

Olivine partial dissolution due to temperature increase and/or decompression, followed by infilling with a melt not necessarily in elemental and isotopic equilibrium with the initial olivine, explains the different major and trace element compositions of OHMIs trapped in a single crystal (e.g., olivines SVN181 from St. Vincent, Ao3-1, Ao15-10 olivines from Aoba in this study, or, for example ARP73-10-03_16, CH77-DR6-203_45 and CH77-DR6-203_55 from Mid-Atlantic Ridge, in Manzini et al., 2019). Such episodes of remobilization or mixing might not always be evident based solely on the major element composition of the olivine, due to fast Fe-Mg diffusion (e.g., Jurewicz and Watson, 1988; Gaetani and Watson, 2002). Thus, local O isotopic equilibrium between the OHMI and the host crystal provides more robust information. Furthermore, if melt inclusions are forming during olivine recrystallization, OHMIs within the same olivine host may not necessarily be trapped at the same P-T conditions even though the olivine is homogeneous in composition.

Another important piece of information is the variability of $\delta^{18}O$, which reflects the influence from different slab components (Bouvier et al., 2019). As OHMIs that have formed in recrystallized olivine record the composition of different melt batches, they could be used to study whether melt batches and slab flux have varied over time. For example, the homogeneity of Vulcano OHMIs and the olivine hosts suggests that the melt batch in equilibrium with the melt inclusions was probably homogeneous. To the contrary, olivines SVN171 and SVN181 from St. Vincent might both have grew in two melt batches with different slab influence: they both contain primitive OHMIs with $\delta^{18}O$ of 6.9‰ in equilibrium with Fo_{83-85}, and more evolved OHMIs with $\delta^{18}O$ at 5.3-5.4‰ surrounded by olivine Fo_{76-77} (see Supplementary Material 1).

6. Conclusions

Oxygen isotopes in olivines and OHMIs in basalts from five volcanoes located in different arcs exhibit a broad range of values that overlap, but with averages that differ from arc to arc. The variability measured in the olivines is not related to the variability measured in the OHMIs that they host. Olivines from four of the five volcanoes record either normal magmatic evolution or magma mixing, based on their Fo and $\delta^{18}O$ compositions. A relatively large proportion of the measurements (70% of XX51 olivine-OHMI pairs) suggest that the OHMIs are not in O isotopic equilibrium with their host, despite their major element compositions being in apparent equilibrium. The O isotopic disequilibrium cannot be explained by temperature variations, as this is not resolvable by SIMS measurements. Trace elements in the OHMIs and their host olivines do not support O isotope disequilibrium being a boundary layer effect. Analysing the olivines in more detail reveals that for most of the olivines at least one O isotope measurement is in equilibrium with each of the OHMIs that it hosts. The olivine domains that are in equilibrium with the OHMI are often <50 μm from the inclusions. It is concluded that these OHMIs were trapped when the olivines were remobilized by melts with different $\delta^{18}O$ compositions or were partly recrystallized during magma mixing. Careful screening of $\Delta^{18}O_{Ol-MI}$, by measuring $\delta^{18}O$ of the melt inclusion and at least 2-4 points in the olivine surrounding the melt inclusions and 2-4 in the olivine core and rim, possibly coupled with phosphorus maps, could open new perspectives: in association with diffusion profile measurements and petrological determination of temperature, it could be used to better understand, for example, melt inclusion formation, crystal history, architecture of magma plumbing systems and variation of slab fluxes.

CRediT authorship contribution statement

Bouvier A.-S.: Data acquisition, Methodology, Validation, Vizualization, Conceptualization, Writing - original draft. Rose-Koga E.F.: Resources, Writing - review & editing. Nichols A.R.L.: Resources, Writing - review & editing. Le Lay C.: Data acquisition, Writing - review & editing.

Declaration of competing interest

The authors declare that they have no known competing financial interests or personal relationships that could have appeared to influence the work reported in this paper.

Acknowledgements

Appendix A. Supplementary material

Supplementary material related to this article can be found online at https://doi.org/10.1016/j.epsl.2022.117638.

References

Auer, S., Bindeman, I., Wallace, P., Ponomareva, V., Portnyagin, M., 2009. The origin of hydrous, high-$\delta18O$ voluminous volcanism: diverse oxygen isotope values and high magmatic water contents within the volcanic record of Klyuchevskoy volcano, Kamchatka, Russia. Contrib. Mineral. Petrol. 157, 209–230. https://doi.org/10.1007/s00410-008-0330-0.

Barnes, J.D., Sharp, Z.D., 2017. Chlorine isotope geochemistry. Rev. Mineral. Geochem. 82, 345–378. https://doi.org/10.2138/rmg.2017.82.9.

Bindeman, I., 2008. Oxygen isotopes in mantle and crustal magmas as revealed by single crystal analysis. Rev. Mineral. Geochem. 69, 445–478. https://doi.org/10.2138/rmg.2008.69.12.

Bindeman, I., Sigmarsson, O., Eiler, J., 2006. Time constraints on the origin of large volume basalts derived from O-isotope and trace element mineral zoning and U-series disequilibria in the Laki and Grímsvötn volcanic system. Earth Planet. Sci. Lett. 245, 245–259. https://doi.org/10.1016/j.epsl.2006.02.029.

Bindeman, I., Gurenko, A., Sigmarsson, O., Chaussidon, M., 2008. Oxygen isotope heterogeneity and disequilibria of olivine crystals in large volume Holocene basalts from Iceland: evidence for magmatic digestion and erosion of Pleistocene hyaloclastites. Geochim. Cosmochim. Acta 72, 4397–4420. https://doi.org/10.1016/j.gca.2008.06.010.

Bouvier, A.-S., Métrich, N., Deloule, E., Metrich, N., Deloule, E., Métrich, N., Deloule, E., Métrich, N., Metrich, N., Deloule, E., Métrich, N., Deloule, E., 2008. Slab-derived fluids in the magma sources of St. Vincent (Lesser Antilles arc): volatile and light element imprints. J. Petrol. 49, 1427–1448. https://doi.org/10.1093/petrology/egn031.

Bouvier, A.-S., Deloule, E., Métrich, N., Metrich, N., 2010. Fluid inputs to magma sources of St. Vincent and Grenada (Lesser Antilles): new insights from trace elements in olivine-hosted melt inclusions. J. Petrol. 51, 1597–1615. https://doi.org/10.1093/petrology/egq031.

Bouvier, A.-S., Manzini, M., Rose-Koga, E.F., Nichols, A.R.L., Baumgartner, L.P., 2019. Tracing of Cl input into the sub-arc mantle through the combined analysis of B, O and Cl isotopes in melt inclusions. Earth Planet. Sci. Lett. 507, 30–39. https://doi.org/10.1016/j.epsl.2018.11.036.

Bucholz, C.E., Jagoutz, O., VanTongeren, J.A., Setera, J., Wang, Z., 2017. Oxygen isotope trajectories of crystallizing melts: insights from modeling and the plutonic record. Geochim. Cosmochim. Acta 207, 154–184. https://doi.org/10.1016/J.GCA.2017.03.027.

Cashman, K.V., Sparks, R.S.J., Blundy, J.D., 2017. Vertically extensive and unstable magmatic systems: a unified view of igneous processes. Science 80, 355. https://doi.org/10.1126/science.aag3055.

Costa, F., Dohmen, R., Chakraborty, S., 2008. Time scales of magmatic processes from modeling the zoning patterns of crystals. Rev. Mineral. Geochem. 69, 545–594. https://doi.org/10.2138/rmg.2008.69.14.

Danyushevsky, L.V., Plechov, P., 2011. Petrolog3: integrated software for modeling crystallization processes. Geochem. Geophys. Geosyst. 12. https://doi.org/10.1029/2011GC003516.

De Hoog, J.C.M., Gall, L., Cornell, D.H., 2010. Trace-element geochemistry of mantle olivine and application to mantle petrogenesis and geothermobarometry. Chem. Geol. 270, 196–215. https://doi.org/10.1016/j.chemgeo.2009.11.017.

Deegan, F.M., Whitehouse, M.J., Troll, V.R., Geiger, H., Jeon, H., le Roux, P., Harris, C., van Helden, M., González-Maurel, O., 2021. Sunda arc mantle source δ18O value revealed by intracrystal isotope analysis. Nat. Commun. 12. https://doi.org/10.1038/s41467-021-24143-3.

Dohmen, R., Chakraborty, S., Becker, H.-W., 2002. Si and O diffusion in olivine and implications for characterizing plastic flow in the mantle. Geophys. Res. Lett. 29, 2030. https://doi.org/10.1029/2002GL015480.

Dorendorf, F., Wiechert, U., Wörner, G., 2000. Hydrated sub-arc mantle: a source for the Kluchevskoy volcano, Kamchatka/Russia. Earth Planet. Sci. Lett. 175, 69–86. https://doi.org/10.1016/s0012-821x(99)00288-5.

Eiler, J., Stolper, E.M., McCanta, M.C., 2011. Intra- and intercrystalline oxygen isotope variations in minerals from basalts and peridotites. J. Petrol. 52, 1393–1413. https://doi.org/10.1093/petrology/egr006.

Eiler, J.M., 2001. Oxygen isotope variations of basaltic lavas and upper mantle rocks. Rev. Mineral. Geochem. 43, 319–364. https://doi.org/10.2138/gsrmg.43.1.319.

Eiler, J.M., Crawford, A., Elliott, T., Farley, K.A., Valley, J.W., Stolper, E.M., 2000a. Oxygen isotope geochemistry of oceanic-arc lavas. J. Petrol. 41, 229–256. https://doi.org/10.1093/petrology/41.2.229.

Eiler, J.M., Schiano, P., Kitchen, N., Stolper, E.M., 2000b. Oxygen-isotope evidence for recycled crust in the sources of mid-ocean-ridge basalts. Nature 403, 530–534.

Foley, S.F., Prelevic, D., Rehfeldt, T., Jacob, D.E., 2013. Minor and trace elements in olivines as probes into early igneous and mantle melting processes. Earth Planet. Sci. Lett. 363, 181–191. https://doi.org/10.1016/j.epsl.2012.11.025.

Gaetani, G.A., Watson, E.B., 2002. Modeling the major-element evolution of olivine-hosted melt inclusions. Chem. Geol. 183, 25–41.

Genske, F.S., Beier, C., Haase, K.M., Turner, S.P., Krumm, S., Brandl, P.A., 2013. Oxygen isotopes in the Azores islands: crustal assimilation recorded in olivine. Geology 41, 491–494. https://doi.org/10.1130/G33911.1.

Gurenko, A.A., Chaussidon, M., 2002. Oxygen isotope variations in primitive tholeiites of Iceland: evidence from a SIMS study of glass inclusions, olivine phenocrysts and pillow rim glasses. Earth Planet. Sci. Lett. 205, 63–79. https://doi.org/10.1016/S0012-821X(02)01005-1.

Gurenko, A.A., Chaussidon, M., Schmincke, H.U., 2001. Magma ascent and contamination beneath one intraplate volcano: evidence from S and O isotopes in glass inclusions and their host clinopyroxenes from Miocene basaltic hyaloclastites southwest of Gran Canaria (Canary island). Geochim. Cosmochim. Acta 65, 4359–4374. https://doi.org/10.1016/S0016-7037(01)00737-2.

Hartley, M.E., Thordarson, T., Taylor, C., Fitton, J.G., EIMF, 2012. Evaluation of the effects of composition on instrumental mass fractionation during SIMS oxygen isotope analyses of glasses. Chem. Geol. 334, 312–323. https://doi.org/10.1016/j.chemgeo.2012.10.027.

Hartley, M.E., Thordarson, T., Fitton, J.G., 2013. Oxygen isotopes in melt inclusions and glasses from the Askja volcanic system, North Iceland. Geochim. Cosmochim. Acta 123, 55–73. https://doi.org/10.1016/j.gca.2013.09.008.

Hofmann, A.W., 1988. Chemical differentiation of the Earth: the relationship between mantle, continental crust, and oceanic crust. Earth Planet. Sci. Lett. 90, 297–314. https://doi.org/10.1016/0012-821X(88)90132-X.

Jochum, K.P., Willbold, M., Raczek, I., Stoll, B., Herwig, K., 2005. Chemical characterisation of the USGS reference glasses GSA-1G, GSC-1G, GSD-1G, GSE-1G, BCR-2G, BHVO-2G and BIR-1G using EPMA, ID-TIMS, ID-ICP-MS and LA-ICP-MS. Geostand. Geoanal. Res. 29, 285–302. https://doi.org/10.1111/j.1751-908X.2005.tb00901.x.

Jochum, K.P., Stoll, B., Herwig, K., Willbold, M., Hofmann, A.W., Amini, M., Aarburg, S., Abouchami, W., Hellebrand, E., Mocek, B., Raczek, I., Stracke, A., Alard, O., Bouman, C., Becker, S., Dücking, M., Brätz, H., Klemd, R., De Bruin, D., Canil, D., Cornell, D., De Hoog, C.-J.J., Dalpé, C., Danyushevsky, L.V., Eisenhauer, A., Gao, Y., Snow, J.E., Groschopf, N., Günther, D., Latkoczy, C., Guillong, M., Hauri, E.H., Höfer, H.E., Lahaye, Y., Horz, K., Jacob, D.E., Kasemann, S.A., Kent, A.J.R.R., Ludwig, T., Zack, T., Mason, P.R.D.D., Meixner, A., Rosner, M., Misawa, K., Nash, B.P., Pfänder, J., Premo, W.R., Sun, W.D., Tiepolo, M., Vannucci, R., Vennemann, T., Wayne, D., Woodhead, J.D., Hofmiann, A.W., Amini, M., Aarburg, S., Abouchami, W., Hellebrand, E., Mocek, B., Raczek, I., Stracke, A., Alard, O., Bouman, C., Becker, S., Dücking, M., Brätz, H., Klemd, R., De Bruin, D., Canil, D., Cornell, D., De Hoog, C.-J.J., Dalpé, C., Danyushevsky, L.V., Eisenhauer, A., Gao, Y., Snow, J.E., Groschopf, N., Günther, D., Latkoczy, C., Guillong, M., Hauri, E.H., Höfer, H.E., Lahaye, Y., Horz, K., Jacob, D.E., Kasemann, S.A., Kent, A.J.R.R., Ludwig, T., Zack, T., Mason, P.R.D.D., Meixner, A., Rosner, M., Misawa, K., Nash, B.P., Pfänder, J., Premo, W.R., Sun, W.D., Tiepolo, M., Vannucci, R., Vennemann, T., Wayne, D.,

Woodhead, J.D., 2006. MPI-DING reference glasses for in situ microanalysis: new reference values for element concentrations and isotope ratios. Geochem. Geophys. Geosyst. 7, Q02008. https://doi.org/10.1029/2005GC001060.

Jurewicz, A.J.G., Watson, E.B., 1988. Cations in olivine, part 2: diffusion in olivine xenocrysts, with applications to petrology and mineral physics. Contrib. Mineral. Petrol. 99, 186–201. https://doi.org/10.1007/BF00371460.

Kent, A.J.R., 2008. Melt inclusions in basaltic and related volcanic rocks. Rev. Mineral. Geochem. 69, 273–331. https://doi.org/10.2138/rmg.2008.69.8.

Koornneef, J.M., Nikogosian, I., van Bergen, M.J., Vroon, P.Z., Davies, G.R., 2019. Ancient recycled lower crust in the mantle source of recent Italian magmatism. Nat. Commun. 10, 1–10. https://doi.org/10.1038/s41467-019-11072-5.

Kress, V.C., Ghiorso, M.S., 1995. Multicomponent diffusion in basaltic melts. Geochim. Cosmochim. Acta 59, 313–324. https://doi.org/10.1016/0016-7037(94)00286-U.

Lacroix, B., Vennemann, T., 2015. Empirical calibration of the oxygen isotope fractionation between quartz and Fe-Mg-chlorite. Geochim. Cosmochim. Acta 149, 21–31. https://doi.org/10.1016/j.gca.2014.10.031.

Lanari, P., Vho, A., Bovay, T., Airaghi, L., Centrella, S., 2019. Quantitative compositional mapping of mineral phases by electron probe micro-analyser. Geol. Soc. (Lond.) Spec. Publ. 478, 39–63. https://doi.org/10.1144/SP478.4.

Lange, A.E., Nielsen, R.L., Iii, F.J.T., Kent, A.J.R., 2013. Diverse Sr isotope signatures preserved in mid-oceanic-ridge basalt plagioclase. Geology 41 (2), 279–282. https://doi.org/10.1130/G33739.1.

Lanzo, G., Di Carlo, I., Pichavant, M., Rotolo, S.G., Scaillet, B., 2016. Origin of primitive ultra-calcic arc melts at crustal conditions - experimental evidence on the La Sommata basalt, Vulcano, Aeolian Islands. J. Volcanol. Geotherm. Res. 321, 85–101. https://doi.org/10.1016/j.jvolgeores.2016.04.032.

Lesher, C.E., 2010. Self-diffusion in silicate melts: theory, observations and applications to magmatic systems. Rev. Mineral. Geochem. 72, 269–309. https://doi.org/10.2138/rmg.2010.72.7.

Lesher, C.E., Hervig, R.L., Tinker, D., 1996. Self diffusion of network formers (silicon and oxygen) in naturally occurring basaltic liquid. Geochim. Cosmochim. Acta 60, 405–413. https://doi.org/10.1016/0016-7037(95)00400-9.

Maclennan, J., 2008. Lead isotope variability in olivine-hosted melt inclusions from Iceland. Geochim. Cosmochim. Acta 72, 4159–4176. https://doi.org/10.1016/j.gca.2008.05.034.

Maclennan, J., McKenzie, D., Grönvold, K., Shimizu, N., Eiler, J.M., Kitchen, N., 2003. Melt mixing and crystallization under Theistareykir, northeast Iceland. Geochem. Geophys. Geosyst. 4. https://doi.org/10.1029/2003GC000558.

Manzini, M., Bouvier, A.-S., Barnes, J.D., Bonifacie, M., Rose-Koga, E.F., Ulmer, P., Métrich, N., Bardoux, G., Williams, J., Layne, G.D., Straub, S., Baumgartner, L.P., John, T., 2017a. SIMS chlorine isotope analyses in melt inclusions from arc settings. Chem. Geol. 449, 112–122. https://doi.org/10.1016/j.chemgeo.2016.12.002.

Manzini, M., Bouvier, A.S., Baumgartner, L.P., Müntener, O., Rose-Koga, E.F., Schiano, P., Escrig, S., Meibom, A., Shimizu, N., 2017b. Weekly to monthly time scale of melt inclusion entrapment prior to eruption recorded by phosphorus distribution in olivine from mid-ocean ridges. Geology 45, 1059–1062. https://doi.org/10.1130/G39463.1.

Manzini, M., Bouvier, A., Baumgartner, L.P., Rose-Koga, E.F., Schiano, P., Shimizu, N., 2019. Grain scale processes recorded by oxygen isotopes in olivine-hosted melt inclusions from two MORB samples. Chem. Geol. 511, 11–20. https://doi.org/10.1016/j.chemgeo.2019.02.025.

Mattey, D., Lowry, D., Macpherson, C., 1994. Oxygen isotope composition of mantle peridotite. Earth Planet. Sci. Lett. 128, 231–241. https://doi.org/10.1016/0012-821X(94)90147-3.

Matthews, A., Stolper, E.M., Eiler, Epstein, S., 1998. Oxygen isotope fractionation among melts, minerals and rocks. In: Goldschmidt Conf. Toulouse, pp. 971–972.

Métrich, N., Deloule, E., 2014. Water content, δD and δ11B tracking in the Vanuatu arc magmas (Aoba Island): insights from olivine-hosted melt inclusions. Lithos 206–207, 400–408. https://doi.org/10.1016/j.lithos.2014.08.011.

Milman-Barris, M.S., Beckett, J.R., Baker, M.B., Hofmann, A.E., Morgan, Z., Crowley, M.R., Vielzeuf, D., Stolper, E., 2008. Zoning of phosphorus in igneous olivine. Contrib. Mineral. Petrol. 155, 739–765. https://doi.org/10.1007/s00410-007-0268-7.

Nichols, A.R.L., Wysoczanski, R.J., Tani, K., Tamura, Y., Baker, J.A., Tatsumi, Y., 2012. Melt inclusions reveal geochemical cross-arc variations and diversity within magma chambers feeding the Higashi-Izu Monogenetic Volcano Field, Izu Peninsula, Japan. Geochem. Geophys. Geosyst. 13, 1–28. https://doi.org/10.1029/2012GC004222.

Paton, C., Hellstrom, J., Paul, B., Woodhead, J., Hergt, J., 2011. Iolite: freeware for the visualisation and processing of mass spectrometric data. J. Anal. At. Spectrom. 26, 2508–2518. https://doi.org/10.1039/c1ja10172b.

Peccerillo, A., De Astis, G., Faraone, D., Forni, F., Frezzotti, M.L., 2013. Compositional variations of magmas in the Aeolian arc: implications for petrogenesis and geodynamics. Geol. Soc. Lond. Mem. 37, 491–510. https://doi.org/10.1144/M37.15 (Chapter 15).

Rose-Koga, E.F., Koga, K.T., Schiano, P., Le Voyer, M., Shimizu, N., Whitehouse, M.J., Clocchiatti, R., 2012. Mantle source heterogeneity for South Tyrrhenian magmas revealed by Pb isotopes and halogen contents of olivine-hosted melt inclusions. Chem. Geol. 334, 266–279. https://doi.org/10.1016/j.chemgeo.2012.10.033.

Rose-Koga, Estelle F., Koga, K.T., Hamada, M., Hélouis, T., Whitehouse, M.J., Shimizu, N., 2014. Volatile (F and Cl) concentrations in Iwate olivine-hosted melt inclusions indicating low-temperature subduction 5. Volcanology geofluid processes in subduction zones and mantle dynamics. Earth Planets Space 66, 1–12. https://doi.org/10.1186/1880-5981-66-81.

Saal, A.E., Hauri, E.H., Langmuir, C.H., Perfit, M.R., 2002. Vapour undersaturation in primitive mid-ocean-ridge basalt and the volatile content of Earth' s upper mantle. Nat. Geosci. 419, 451–455.

Sharp, Z.D., 1990. A laser-based microanalytical method for the in situ determination of oxygen isotope ratios of silicates and oxides. Geochim. Cosmochim. Acta 54, 1353–1357. https://doi.org/10.1016/0016-7037(90)90160-M.

Sorbadere, F., Schiano, P., Métrich, N., Garaebiti, E., 2011. Insights into the origin of primitive silica-undersaturated arc magmas of Aoba volcano (Vanuatu arc). Contrib. Mineral. Petrol. 162, 995–1009. https://doi.org/10.1007/s00410-011-0636-1.

Sparks, S.R.J., Sigurdsson, H., Wilson, L., 1977. Magma mixing: a mechanism for triggering acid explosive eruptions. Nature 267, 315–318. https://doi.org/10.1038/267315a0.

Stracke, A., Genske, F., Berndt, J., Koornneef, J.M., 2019. Ubiquitous ultra-depleted domains in Earth's mantle. Nat. Geosci. 12, 851–855. https://doi.org/10.1038/s41561-019-0446-z.

Wang, Z., Eiler, J., 2008. Insights into the origin of low-δ18O basaltic magmas in Hawaii revealed from in situ measurements of oxygen isotope compositions of olivines. Earth Planet. Sci. Lett. 269, 377–387. https://doi.org/10.1016/j.epsl.2008.02.018.

Warden, A.J., 1970. Evolution of Aoba caldera volcano, New Hebrides. Bull. Volcanol. 34, 107–140. https://doi.org/10.1007/BF02597781.

Wieser, P.E., Edmonds, M., Maclennan, J., Jenner, F.E., Kunz, B.E., 2019. Crystal scavenging from mush piles recorded by melt inclusions. Nat. Commun. 10. https://doi.org/10.1038/s41467-019-13518-2.

Zheng, Y.F., Metz, M.S., Sharp, Z.D., 1999. Oxygen isotope exchange processes and disequilibrium between calcite and forsterite in an experimental C-O-H fluid. Geochim. Cosmochim. Acta 63, 1781–1786. https://doi.org/10.1016/S0016-7037(99)00127-1.